Flux-Assisted Gas Tungsten Arc and Laser Welding of Titanium with Cryolite-Containing Fluxes: Arc **Spectroscopy and Corrosion Resistance Studies**

Arc temperature and arc force were found to contribute to deeper weld penetration in flux-assisted gas tungsten arc welding

BY T. ALSABTI, A. ALSHAWAF, AND S. LIU

ABSTRACT

This research compares autogenous welding, welding with a solid welding wire, and welding with tubular welding wires on CP-titanium using gas tungsten arc (GTA) and laser beam (LB) welding. Commercially pure titanium (CP-Ti Grade 2) solid wire and two newly designed flux-cored tubular wires containing cryolite (Na₃AlF₆) and MgF₂ were used. The comparison covers the aspects of weld penetration, arc constriction, arc force, arc emission spectral lines, arc temperature, and constituent concentrations in the arc. Laser beam welding was performed for comparison since it does not involve arc plasma as in the GTAW process. Also, this research investigated two mechanisms for weld penetration, arc constriction, and Marangoni convection, which were suggested in previous literature as the driving mechanisms for the deeper weld penetration observed with the use of fluxes. Flux-assisted gas tungsten arc welding is also known as activated tungsten inert gas (A-TIG) welding. This work concluded that mainly arc temperature and arc force contributed to the deeper weld penetration. Surface-tension-driven flow (Marangoni convection) was found not to contribute to the weld penetration increase observed with increasing cryolite content. Immersion corrosion test results on the A-TIG weld specimens in separate 3.5% sodium chloride (NaCl) and 0.1% phosphoric acid (H₃PO₄) solutions for 800 h, particularly in terms of mass loss, compared favorably with the autogenous welds.

KEYWORDS

- Gas Tungsten Arc Welding (GTAW) A-TIG
- Cryolite-Containing Fluxes Marangoni Convection
- Laser Beam Welding Arc Spectrometer Immersion Corrosion Test

Introduction

The use of titanium alloys has been expanding in the aerospace, powergeneration, medical, chemical plants, and marine applications due to their

superior mechanical and corrosion properties. The main welding process for titanium alloys is gas tungsten arc welding (GTAW), also known as tungsten inert gas (TIG) welding. The major shortcomings of the GTAW

process, even though it produces highquality welds, are the slow production rate and shallow weld penetration. Single-pass welds with GTAW can have around 2-3 mm penetration creating a bottleneck in the fabrication process (Refs. 1, 2). In the 1960s, researchers at the E. O. Paton Institute invented the A-TIG process for welding titanium alloys by using oxygen-free activated fluxes that significantly increased weld penetration (Refs. 3, 4). The observed deep penetration was attributed to arc constriction and increase in current density. Fluorides of alkali and alkali/earth metals were found to be effective in increasing weld penetration in titanium alloys with observation of arc constriction (Refs. 5, 6).

Welding arc plasma is complex and difficult to investigate. One of the better techniques that can determine the concentrations of arc constituents and estimate arc temperature is arc emission spectroscopy. The concept of arc spectroscopy is to measure the intensity (emission coefficient) of the light (at specific wavelengths) emitted by the arc plasma. An atom, an ion, or electrons at high temperature will become excited, shifting from one energy state to another of higher energy, e.g., from L shell to M shell in the case of the electrons. Following the excitation process, the metastable particles decay, dropping from the higher energy state to a lower energy state. Under set conditions, the decay of an electron from a shell at a higher energy state (E1) to a lower energy shell (E2), as shown in Fig. 1, will be accompa-

T. ALSABTI is with Consulting Services Department, Saudi Aramco, Kingdom of Saudi Arabia. A. ALSHAWAF is with Saudi Basic Industrial Corp. (SABIC), Al Jubail, Kingdom of Saudi Arabia. S. LIU is with Colorado School of Mines, Center for Welding, Joining and Coatings Research, Golden, Colo.

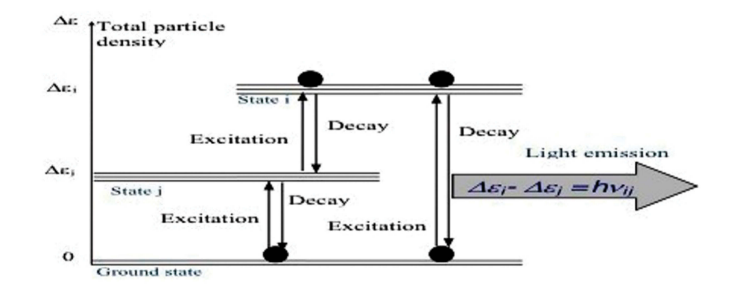


Fig. 1 - Illustration of excitation and decay of electron in energy states in electronic structure in atoms or ions (Ref. 7).



Fig. 3 — Arc constriction observed in the GTA and A-TIG welds.

nied by the emission of a monochromatic light according to the following equations (Refs. 7, 8):

$$E_1 - E_2 = \Delta E = hv \tag{1}$$

$$c = v\lambda$$
 (2)

where ΔE is the change in energy, h is Planck's constant, v is the frequency of the emitted light, λ is the wavelength, and c is the speed of light. The emitted light will have a specific wavelength as determined by the energy change associated with the electron during its

decay. Each decay event in a given atom has a characteristic wavelength of light associated with it. It is the unique emitted spectra by certain

decay events that allow for detection of the elements within an arc.

It has been shown by Bang, Chirieleison, and Liu (Ref. 1) that increasing amounts of a simple fluoride, MgF₂, both in paste and flux cored wire form, increased weld bead pene-





Fig. 2 — As-welded GTA (autogenous and solid wire) and A-TIG welds (Wires 15 and 45).

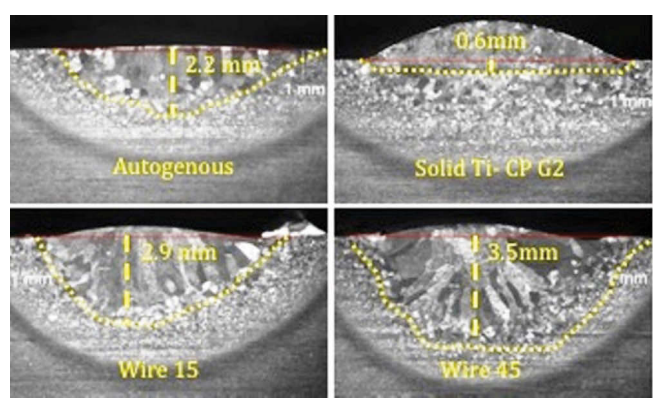


Fig. 4 — Cross-section macrograph of the GTA and A-TIG welding.

tration in titanium by nearly 200% over fluxes without the fluoride. In their work, MgF₂ was used as an addition into CaF₂, BaCl₂, AlF₃, and NaF. The mechanism in this case was attributed to arc constriction. They explained that as the amount of flux vapor entering the weld zone increases, the thermal conductivity of the arc increases and the arc constricts. This explanation was supported by research conducted by Zamkov, Prilutsky, and Gurevich (Ref. 5). In addition, the electrical conductivity of the arc will decrease with an increase in flux vapor due to the trapping of electrons in the outer peripheral region of the arc. In this region, temperatures are generally not high enough to fully dissociate atoms into ions. The flux vapor exists as molecules that can attract free electrons to form negatively charged particles. The degree of arc constriction will then depend on how effectively the vaporized molecules can trap these electrons. Bang, Chirieleison, and Liu (Ref. 1) also noticed the presence of titanium spectra lines when welding with MgF₂-containing fluxes. Without the addition of MgF₂, the spectra lines of

Table 1 —GTA Welding Parameters

GTA Welding Parameters

MachineMiller Dynasty 350 (GTA)Current180 ATravel Speed3 mm/sShielding Gas Type and FlowArgon (UHP G5.0), 0.275 L/sElectrode Type and Size2% Thoriated, 3.2 mmElectrode Tip Preparation45-deg included angleArc Length5 mm

Table 2 — Laser Welding Parameters

Laser Welding Parameters

Type/Mode Power/Focus Travel Speed Shielding Gas Type and Flow Wire Feed Rate Yb-Fiber Laser continuous wave mode/ Conduction mode 1100 W/5 mm (under plate surface) 3 mm/s
Argon (UHP G4.5), 0.157 L/s
13 mm/s (Solid CP Ti-G2 wire)
4 mm/s (Wires 15 & 45)

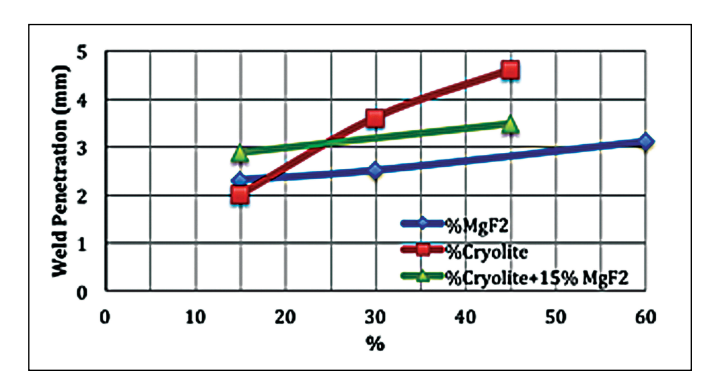


Fig. 5 — Weld penetration comparison for different fluoride flux systems.

titanium were absent. Hillier, Liu, and Roepke (Ref. 2) investigated the effects of cryolite, which contains more F⁻ ions in its formula than MgF₂. Compared to MgF₂ flux pastes, welds using cryolite pastes proved to be more effective, netting up to two times deeper penetration and depthto-width ratio. Thus, cryolite can be considered a strong ingredient in an activating flux.

This work attempted to characterize the effects of cryolite and distinguish the effects of arc constriction, arc force, and Marangoni convection on Ti weld penetration. Parallel to the welding study, a corrosion study was also carried out to determine the corrosion resistance of these A-TIG welds by comparing them to the autogenous welds and base metal.

Experimental Procedure

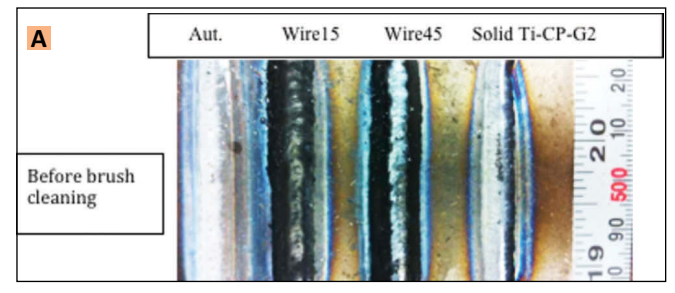
Welding experiments were conducted to examine the effects of selected fluxes on penetration in commercially-pure titanium (CP-Ti). Commercially-pure titanium (Grade 2) solid wire and two tubular cored wires containing cryolite in different proportions [15% (Wire 15) and 45% (Wire 45)] in a base flux that contained 15% MgF₂ were manufactured and tested. CaF₂, BaCl₂, AlF₃, and NaF were the remaining ingredients in the fluxes. Autogenous GTAW was done as reference (Table 1). Comparison between these two sets of welds would clarify the effects of the activating flux on weld penetration. Aside from A-TIG, laser beam welding (LBW) was also done (Table 2). Since LBW does not involve any significant arc plasma, it was hoped comparison

es would elucidate the effects of arc plasma on weld penetration. An Ocean Optics USB 4000 spectrometer was used to record the arc emission wavelengths and relative intensities. The arcs were also photographed for subsequent analysis. The detector range was between 200 and 1100 nm. The collimating lens size was 5 mm. Other experimental data are listed in Table 3.

of the two process-

4.5 Weld Penetration (mm) 4 3.5 3 2.5 15% Cryolite+70% 2 1.5 1 0.5 3.2 4.8 3.4 3.8 4.4 4.6 Arc Force (10⁻³ N)

Fig. 6 — Arc force vs. weld penetration.



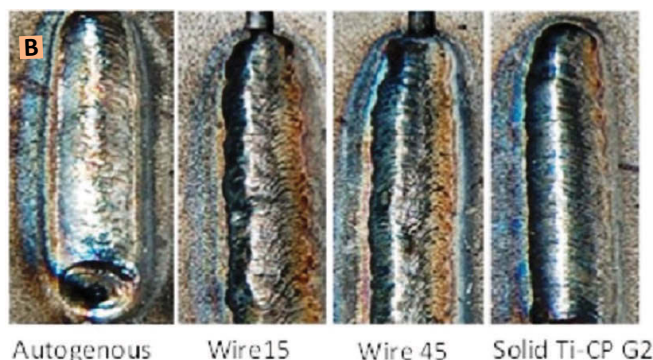


Fig. 7 — As-welded condition with the laser welding process.

Results and Discussion

Results of GTAW Experiments

The as-welded GTA and A-TIG welds are shown in Fig. 2. The welds in general showed good bead morphology. Some evidence of oxidation and ni-

Table 3 — Experimental Data

Plate Thickness 5.1 mm Wire Diameter 1.57 mm Wire Feed Rate 13 mm/s (Solid CP Ti-G2 wire) 4 mm/s (Wires 15 & 45) Position of Feed Introduced into the front of arc

trogen pickup can also be seen indicating that impurities such as oxygen and nitrogen may be present and negatively affect the mechanical and corrosion properties of the A-TIG welds. The immersion corrosion test results are discussed at the end of this section.

The arc plasmas for the autogenous, Wire 15, and Wire 45 welds were pho-

Table 4 — Arc Constriction Data for the **Experimental Welds**

Weld Case	Arc Constriction $\%$		
	Area Method	Line Method	
Autogenous	0	0	
Wire 15	21.0	7.5	
Wire 45	5.5	0	

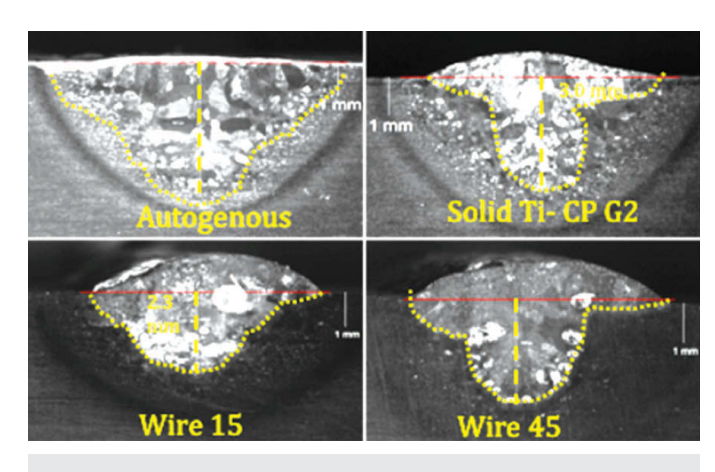


Fig. 8 — Cross-section macrograph of the laser welding process.

Table 5 — Weld Penetration Data for the Experimental Welds

Weld Case	Width (mm)	Penetration Depth, mm
Autogenous	5.5	2.2
Ti-CP G2	7.0	0.6
Wire 15	6.0	2.9
Wire 45	7.1	3.5

Table 6 — Weld Penetration for Laser Welding Process

Width (mm)	Penetration Depth (mm)
7.5	3.9
5.4	3.0
4.8	2.3
5.5	2.7
	7.5 5.4 4.8

tographed for comparison, as shown in Fig. 3. Arc constriction was measured by two methods. The first was measuring the area of the cross section of the arc, as marked in Fig. 3. The second method measured the length of the horizontal line, i.e., the arc width, in the middle of the arc length. Wire 15 showed greater arc constriction than Wire 45 in both methods, as shown in Table 4. Wire 15 exhibited 21% arc constriction as compared to 5.5% for Wire 45 in the area measurement method. Using the line measurement method, Wire 15 showed 7.5% arc constriction whereas no arc constriction was observed for Wire 45.

The welds were cross sectioned, polished, and etched to measure the weld penetration, as shown in Fig. 4. Kroll's reagent, containing 6 vol-% HNO₃, 2 vol-% HF, and 92 vol-% distilled water, was used for etching. The weld penetration for each case was

measured and recorded in Table 5. Wire 45 was found to have produced

the highest weld penetration of 3.5 mm followed by Wire 15 of 2.9 mm. The autogenous weld penetration measured only 2.2 mm. So, as the content of the complex fluoride (cryolite) increased, the weld penetration also increased, which confirmed research work by Hillier et al. (Ref. 2).

Figure 5 shows a summary of weld penetration of this research work using A-TIG wires (15% and 45% cryolite + 15% MgF₂), the A-TIG wires (15, 30, 45, and 60% cryolite) reported by Hillier et al. (Ref. 2), and the A-TIG wires (15, 30, and 60% MgF₂) from the research work of Bang, Chirieleison, and Liu (Ref. 1). The weld penetration of Wire 15 (combined 15% cryolite and 15% MgF₂) was higher than the 15% MgF₂ and 15% cryolite, respectively. On the other hand, the weld penetration of 30% cryolite was higher by around 1 mm than the 30% MgF₂ weld. Also, the weld penetration of 45% cryolite is much higher than Wire 45 (45% cryolite + 15% MgF₂) and 60% MgF₂, respectively. Thus, increases in Na₃AlF₆ played a definite role in penetration. Overall, mixed Na₃AlF₆ plus MgF₂ fluxes increased penetration over the MgF₂ addition alone, but did not promote deeper penetration than single cryolite or magnesium fluoride additions at higher concentrations. Cryolite promoted greater penetration than the other flux ingredients when added at 30 and 45%.

Effect of Arc Force

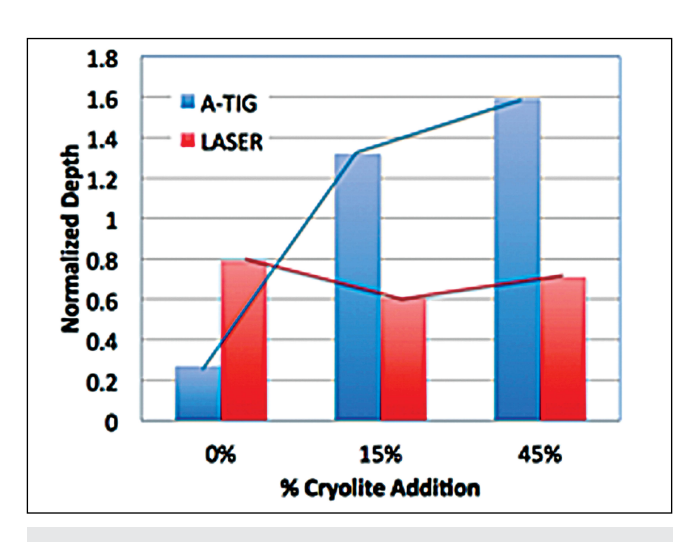


Fig. 9 — Variation of the weld depth-to-autogenous weld depth ratio as a function of cryolite addition in the flux.

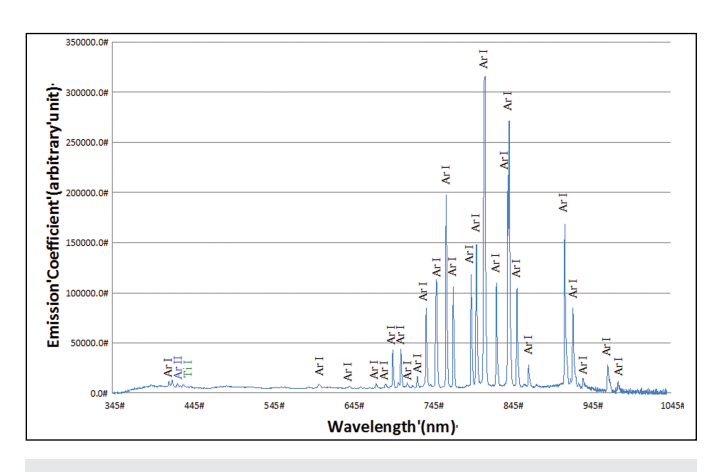
The arc force mechanism was investigated by measuring the R2/R1 ratios from the photographed arcs of the autogenous, Wire 15, and Wire 45 welds from this research work as well as the arcs from the welds by Hillier et al. The R2/R1 ratios were calculated by using the following arc force equation (the equation Converti) (Refs. 8–10):

$$F = \frac{\mu_0 I^2}{8\pi} \left(1 + 2\ln\frac{R_2}{R_1} \right) \tag{3}$$

where I is the welding current, μ_0 is the permeability of free space, R_1 is the radius of the arc where it contacts the welding electrode, R_2 is the radius of the arc where it contacts the base plate. The arc force was plotted vs. the weld penetration of each case in Fig. 6. Despite the scatter in the data, a clear relationship can be seen between arc force and weld penetration. Increasing arc force increased weld penetration. This finding is contrary to the results reported by Burleigh and Eagar (Ref. 11) who did not find any correlation between the arc forces and weld penetration of several flux systems (Refs. 12-15).

Results of Laser Welding Process Experiments

The welds made by the laser welding process in conduction mode are shown in Fig. 7. The laser welding process was chosen to eliminate the effect of arc



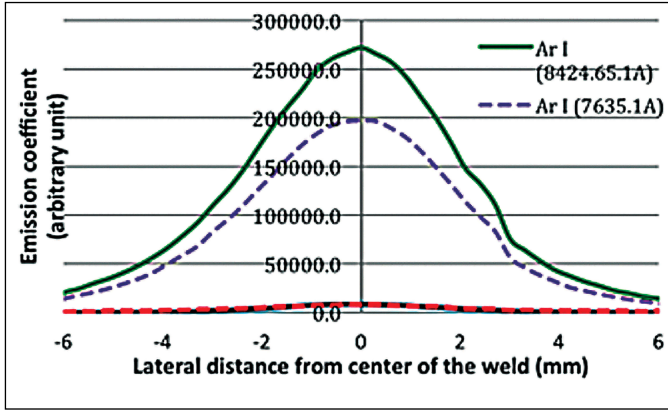
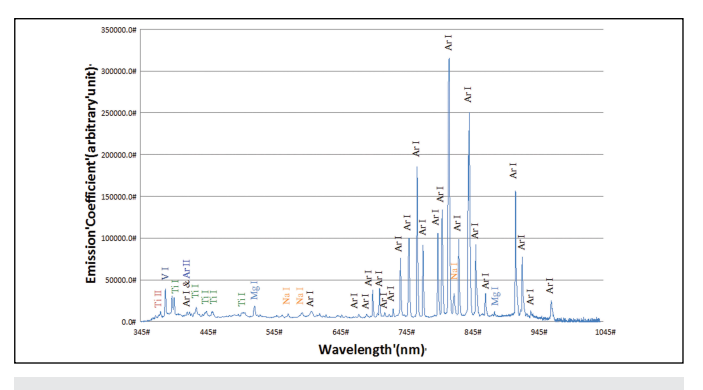


Fig. 10 — Emission spectral line peaks from autogenous weld.

Fig. 11 — Major spectra peaks across autogenous weld.



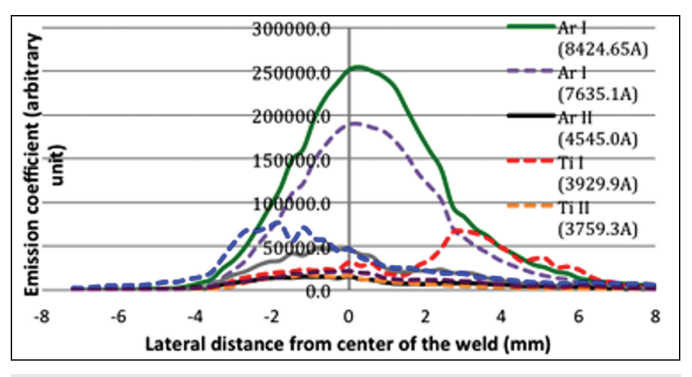


Fig. 12 — Emission spectral line peaks from Wire 15 weld.

Fig. 13 — Major spectra peaks across Wire 15 weld.

constriction in an attempt to clarify whether Marangoni convection is present in these welds. Increasing weld penetration in these experiments would indicate a contribution of surface-tensiondriven flow. The consumable in the form of a wire was laid on top of the plate prior to laser irradiation. The laser beam was then rastered over the wire and the plate. Total melting of the wire and wetting of the plate was observed. The welds were sectioned, polished, and etched, and the cross sections are shown in Fig. 8.

Table 6 lists the weld penetration of each case. It was observed that the weld made using Wire 45 had slightly deeper penetration (2.7 mm) than the Wire 15 weld (2.3 mm). However, weld penetrations that resulted from both of the A-TIG wires were lower than those of the solid Ti-CP G2 wire (3.0 mm) and the autogenous laser weld (3.9 mm). The reason for having lower weld penetration for all three wires than for the autogenous laser weld is likely because of the placement of the wire on top of the test plate. By positioning the wire on top of the test plate, most of the laser

power was consumed in the melting of the wire and little was left for the melting of the base plate to form the weld pool, thus the shallower welds. It also appeared that the flux cored wires absorbed more energy from the laser beam than the solid wire, which would explain why the A-TIG welds have lower weld penetration than the solid Ti-CP G2 wire.

Figure 9 shows the calculated weld depths normalized by the autogenous weld depth for both A-TIG and laser welding. The normalized depths for the laser welding remained practically unchanged despite increasing cryolite content. Contrarily, the A-TIG welds showed normalized weld depths increase with increasing cryolite addition. Thus, it can be concluded that Marangoni convection did not have any significant contribution as a driving mechanism in increasing weld penetration. This finding is supported by the findings of Howes and Lucas (Ref. 16). Using A-TIG pastes for stainless steel by laser and electron beam welding, they concluded that A-TIG fluxes are effective only for welds done by arc and plasma welding processes.

Temperature and Concentration Calculation Results

The spectral lines data collected by arc spectrometer from the autogenous GTA weld, and the A-TIG welds with Wires 15 and 45 were processed and mapped in Figs. 10-14. Using a Mathematica program, the spectral line emission data collected from each weld case were processed and used to determine the temperature of the arc and the concentrations of arc constituents by the off-axis peak method (Fowler-Milne Method). The asymmetrical behavior in the spectral peaks in these figures is most likely due to the single scanning of the arc position. The emission data were collected from individual slices of the arc along the line of sight of the spectrometer. Note that continual scanning of the entire cross section of the arc would have allowed for the Abel Inversion calculation and captured the entire arc emission signals to result in a more symmetrical distribution in the spectral peaks.

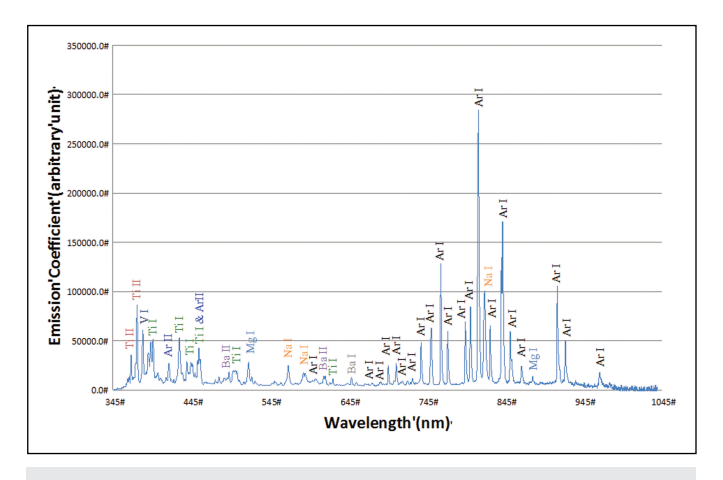


Fig. 14 — Emission spectral line peaks from Wire 45 weld.

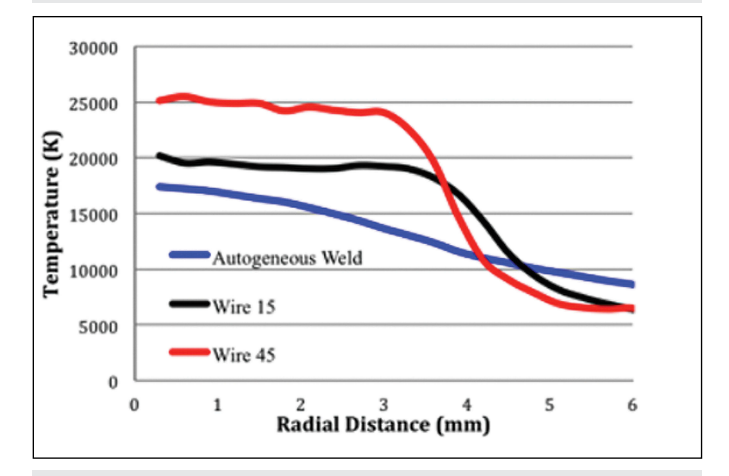


Fig. 16 — Arc temperature profile.

However, single scans like the ones described in this work are still useful to gain insight to the arc during titanium welding. Neutral argon (Ar I) spectral lines were dominant for the autogenous welding arc, as indicated in Fig. 8. In addition, very low intensity spectral lines of ionized argon (Ar II) and titanium vapor (Ti I) are visible in Figs. 10 and 11. Despite the molten titanium weld pool, little titanium vapor was absorbed above the weld. Figure 11 plots the emission coefficients for specific wavelengths for Ar I from one edge of the arc to the other. In comparison, Wire 15 has more spectral lines for other constituents such as first ionized titanium (Ti II), neutral vanadium (V I), neutral sodium (Na I), and neutral magnesium (Mg I), as shown in Figs. 12 and 13.

Spectral lines of other constituents such as neutral aluminum (Al I) might be hidden behind the lines of the other elements mentioned earlier. This

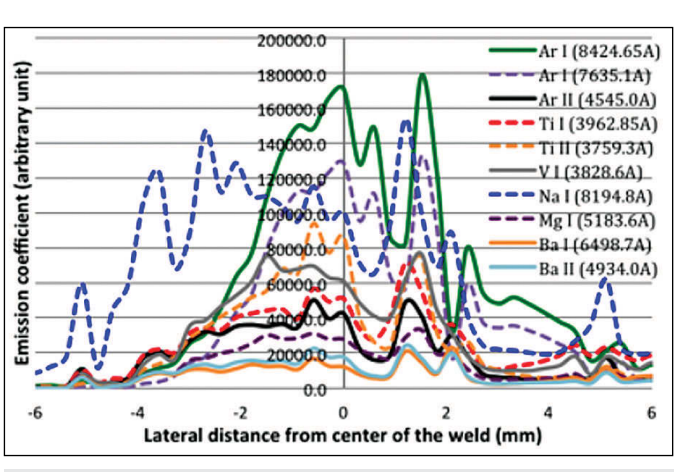


Fig. 15 — Major spectra peaks across Wire 45 weld.

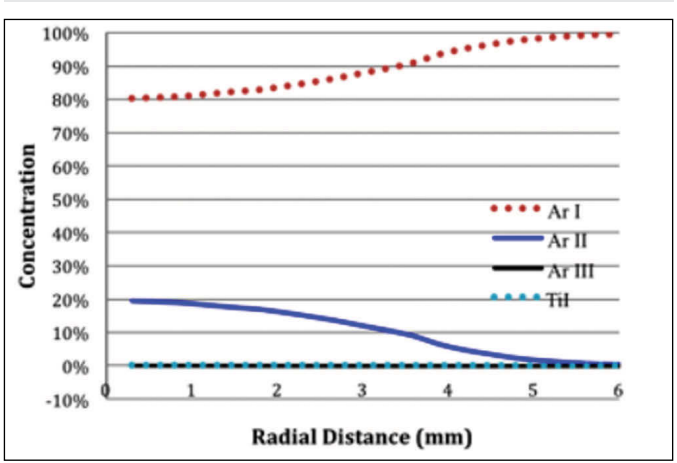
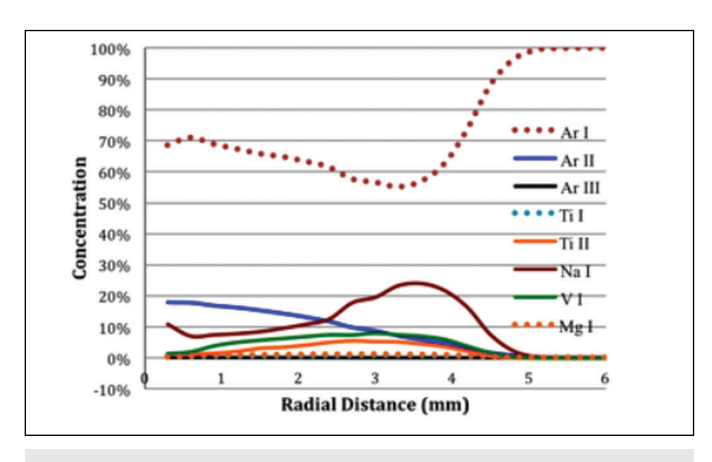


Fig. 17 — Autogenous welding arc constituent concentrations.

limitation is partly due to the low resolution of the specific arc spectrometer used. The collimating lens size of 5.0 mm was much larger than the condition of "not more than 0.25 mm" that Hiraoka (Ref. 17) had suggested in order to limit the error of line intensities within 3%. The spectral lines of fluorides were difficult to observe because of their higher energy levels and that the transition probabilities are lower than those of metallic constituents such as magnesium or sodium. As for Wire 45, more constituents are found in the arc as well as higher intensities as shown in Figs. 14 and 15. First ionized titanium (Ti II) lines were noticed and they had higher intensity than the neutral titanium (Ti I) lines. Also, neutral sodium (Na I) lines were increased across the weld in general. The neutral sodium came mainly from the dissociation of cryolite (Refs. 18-20). The asymmetric distribution of the

different species, e.g., Ar I and Na I, is a reflection of the fact that spectral data collection was from a slice of the arc and not considering the entire arc column. (Refs. 21–23).

Figure 16 shows the arc temperature of each weld case. At the center of the weld, the autogenous welding arc had the lowest temperature of around 17,500 K. The Wire 15 welding arc temperature was approximately 2800 K higher at the center of the arc and the weld penetration was around 0.6 mm deeper than the autogenous welds. The Wire 45 welding arc was approximately 5000 K higher than the Wire 15 arc and the weld penetration was around 0.6 mm deeper. A possible explanation for this behavior is the greater contribution of arc temperature observed in Wire 45. The arc force calculated for the two welding wires were quite similar, 0.0042 N for Wire 15 and 0.0045 N for Wire 45, implying that the



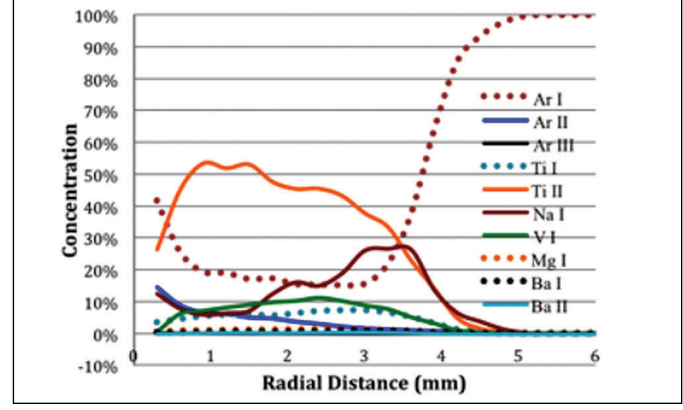


Fig. 18 — Wire 15 welding arc constituent concentrations.

Fig. 19 — Wire 45 welding arc constituent concentrations.

Table 7 — Comparison between Wires 15 and 45

	Wire 15	Wire 45
Arc Constriction	21%	5.5%
Arc Force	0.0042 N	0.0045 N
Arc Temperature	20177 K	25177 K
Weld Penetration	2.9 mm	3.5 mm
(A-TIG)		
Weld Penetration	2.3 mm	2.7 mm
(Laser)		

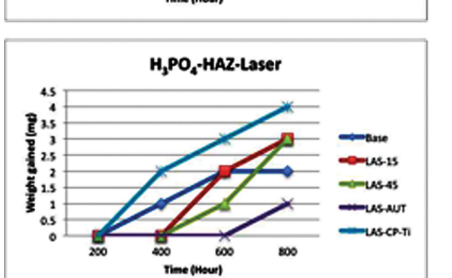
Table 8 — Corrosion Rate Based on Equation 4 in mm/year

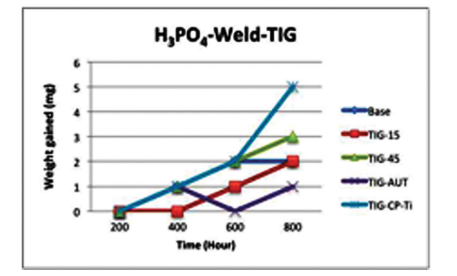
iii iiiii, yeai			
Base Plate	0.1% H ₃ I 0.1	PO ₄	3.5% NaCl 0.05
	HAZ	Weld	HAZ
GTAW-AUT	0.1	0.1	0.1
GTAW-Ti-CP G2	0.2	0.2	0.1
A-TIG-45	0.2	0.2	0.1
A-TIG-15	0.2	0.2	0.1
LAS-Ti-CP G2	0.2	0.2	0.1
LAS-AUT	0.1	0.1	0.1
LAS-45	0.1	0.2	0.1
LAS-15	0.2	0.1	0.1

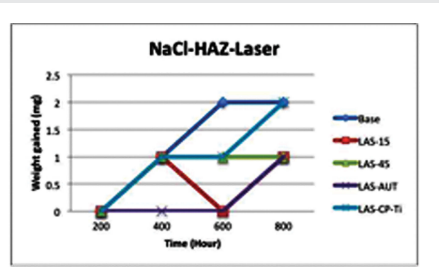
contribution of arc force in weld depth for these two welds would be similar. As for concentrations of the arc constituents, the autogenous weld contained approximately 80% neutral argon (Ar I) and 20% first ionized argon (Ar II) in the center of the weld. The second ionized argon (Ar III) and neutral titanium (Ti I) made up about 0.2% of the arc in the center of the weld, as shown in Fig. 17. The neutral argon (Ar I) percentage in the arc increased with increasing distance from the center of the arc — Fig. 17. The first ionized argon (Ar II) decreased gradually until 3.6 mm away from the center of the arc.

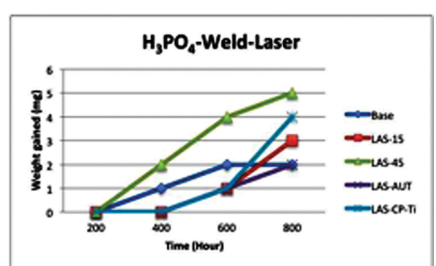
The concentration of the con-

NaCI-HAZ-TIG 2.5









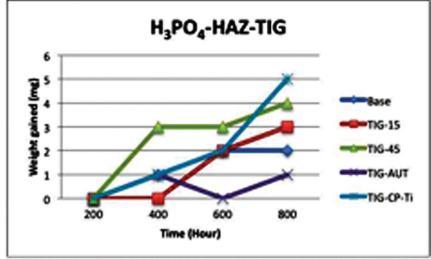


Fig. 20 — The average mass gain in both solutions compared to the titanium base plate.

stituents of the Wire 15 arc (Fig. 18) shows decreasing neutral argon concentration from 70% at the center of the weld to 55% at 3.3 mm away from the center, mainly due to the increase of neutral sodium to around 24%. At distances greater than 5.0 mm from the center of the arc, only Ar I was observed. The concentrations of neutral and first ionized titanium, neutral vanadium, and neutral magnesium all increase in the core of the arc. The concentration of the first

ionized titanium also increased to 5.5% as compared to 0.6% concentration of neutral titanium. The arc data on ionized titanium support the higher calculated arc temperatures. The Wire 45 weld (Fig. 19) shows a larger number of constituents present and higher concentration percentages for the metallic constituents in the arc than Wire 15 (Table 7). Neutral and first ionized barium were also observed in the arc due to its high temperature (Refs. 24, 25).

Immersion Corrosion Test of Titanium in NaCl and H₃PO₄ Environment at 25°C

The corrosion resistance of titanium is based on the presence of a stable, continuous, and adherent oxide layer. This layer forms spontaneously and immediately upon exposure to oxygen. If damaged, it re-forms readily as long as there is some source of oxygen (air or moisture) in the environment (Ref. 26).

The immersion corrosion test was conducted according to NACE TM0169/G31-12a. Samples were extracted from both the laser and GTA welding processes and then prepared by grinding on No. 120 abrasive SiC paper. Each zone of the weld was studied separately because some welds may be cathodic or anodic to the base metal and may affect the corrosion rate. Corrosion of welded specimens is normally localized and not representative of the entire surface. The test duration was 800 h. Samples were weighed using an electronic analytical balance. The weights of polished and dried samples before immersion and washed and dried samples after immersion were measured and the mean values determined. All samples gained mass because of the titanium oxide formation. The average mass gain is 2 to 5 mg depending on the solution, as shown in Fig. 20. The corrosion rates of the samples were also calculated using the following equation:

Corrosion rate = $(K \times W)/(A \times T \times D)$ (4)

where K is a constant equal to $8.76 \times$ 10⁴, T is time of exposure in hours, A is area in cm², W is mass loss in grams, and D is density ($Ti = 4.54 \text{ g/cm}^3$). The corrosion rates calculated according to this equation for titanium in sodium chloride solution and in phosphoric acid solution are shown in Table 8. As a result of the sample mass gain, the corrosion products of the titanium must have deposited and attached on the Ti sample surface. The above results seem to corroborate the formation of titanium oxide phosphate on titanium surface in phosphoric acid. This observation is supported by a number of experimental results in literature as follows: by nuclear reaction analysis, Ferdjani et al. (Ref. 27) found phosphate incorporation in titanium oxide formed by anodization in 3.0~mol/L H_3PO_4 solution; by qualitative EDS analysis, Krasicka-Cydzik (Ref. 28) found titanium phosphate deposit in the form of an amorphous thin layer in anodized commercially pure titanium in 0.5~mol/L phosphoric acid; by FT-IR study, Narayanan et al. (Ref. 29) also showed the presence of titanium oxide phosphate in the titanium surface anodized in 0.3~mol/L phosphoric acid.

From the experiments, the corrosion resistance of the titanium base plate and all laser and GTA welded titanium samples was higher in the NaCl solution than in the H₃PO₄ solution. The mass gain in the NaCl solution was around 2 mg while it was around 5 mg in the H₃PO₄. It was noticed that GTA welded Ti-CP G2 samples had the highest mass gain (~ 5 mg) in the H₃PO₄ solution followed by the fluoride-containing wires and then the base plate with the autogenous weld samples. The mass gain for the laser weld and heat-affected zone samples for Ti-CP G2 was about 4 mg while it reached 5 mg when GTAW was used. It was noticed previously in the GTA and laser welding discussion sections that the solid wire (Ti-CP G2) absorbed more energy (compared to the flux cored wires) from the laser beam to result in deeper penetration. Less penetration resulted from the GTAW process. It seems that the level of energy absorption from both welding processes does not much affect the corrosion resistance of the solid wire (Ti-CP G2). Rather, it is more related to the chemical composition and the purity of the alloy grade. In general, the higher the purity of CP Ti, the greater the corrosion resistance. The solid wire Ti-CP G2, with very low impurity levels, has been widely used because it is capable of performing well in many critical corrosion applications such as marine environments and chemical processing. In seawater, it is fully resistant to corrosion at temperatures up to 315°C (600°F) (Ref. 30). Hence, A-TIG welds showed a slightly higher corrosion rate than the laser welds. The autogenous welds in both welding processes showed the lowest corrosion rate. It can be concluded that the corrosion resistance of the welds produced with Wires 45 and 15 are higher than those with Ti-CP G2.

Conclusion

Arc constriction, arc force, and arc temperature are confirmed to be the driving mechanisms of the A-TIG welding process. As the cryolite content in the flux increases, the weld penetration, arc force, and arc temperature increase as well. The increase in arc temperature led to increases in arc constituent concentrations. The arc constricts with the increase of cryolite content in the flux up to a certain percentage and then decreases with further cryolite addition. Comparison between the depths of the activated and autogenous welds showed Marangoni convection does not have a significant contribution as a driving force in the weld penetration. It was found that arc constriction and arc temperature are the two dominant driving mechanisms in weld penetration for fluxes of lower cryolite contents. As for fluxes with higher cryolite contents, the arc temperature is the main mechanisms for weld penetration. Finally, Wires 45 and 15 produced welds with much better corrosion resistance than Ti-CP G2. For all three wires and autogenous welds, the phosphoric acid solution caused greater corrosion than the sodium chloride solution.

References

- 1. Bang, K. S., Chirieleison, G., and Liu, S. 2005. Gas tungsten arc welding of titanium using flux cored wire with magnesium fluoride. *Science and Technology of Welding and Joining* 10(5): 617–623.
- 2. Hillier, C., Liu, M., Roepke, C., and Liu, S. 2009. A-TIG welding of CP titanium plates using cryolite-containing flux pastes and flux-cored wires. *Proceeding of the AWS Welding Show*, Chicago, Ill.
- 3. Howse, D. H., and Lucas, W. 2000. An investigation into arc constriction by active fluxes for TIG (A-TIG) welding. *Science and Technology of Welding and Joining* 5(3): 189–193.
- 4. Kumar, V., Lucas, B., Howse, D., Melton, G., Raghunathan, S., and Vilarinho, L. O. 2009. Investigation of the A-TIG mechanism and the productivity benefit in TIG welding. Proceedings of the 15th International Conference on the Joining of Materials and 6th International Conference on Education in Welding, Helsing@r, Denmark.
 - 5. Gurevich, S. 1970. U.S. Patent

3,551,218.

- 6. Liu, S., and Perez, F. 2001. Manufacturing titanium flux-cored arc welding electrodes — Feasibility study. U.S. Navy Contract N00167-01-M-0053, Final report.
- 7. Chandler, J. H. 2004. Spectroscopic monitoring of hydrogen in welding arcs. Colorado School of Mines, Golden, Colo., master's thesis.
- 8. Converti, J. 1981. MIT, Cambridge, Mass., PhD thesis, mechanical engineering, p. 57.
- 9. Modenesi, P. J., Apolinario, E. R., and Pereira, I. M. 2000. TIG welding with single-component fluxes. Journal of Materials Processing Technology, pp. 99, 260-265.
- 10. Lucas, W., and Howse, D. 1996. Activating flux — Increasing the performance and productivity of the TIG and plasma processes. Welding and Metal Fabrication 64(1): 11-17.
- 11. Burleigh, T. D., and Eagar, T. W. 1983. Measurement of the force exerted by a welding arc. Metallurgical Transactions A 14A: 1223, 1224.
- 12. Chirieleison, G. M. 2004. The effect of flux ingredients on flux-cored arc welding on titanium. Colorado School of Mines, Golden, Colo., MS thesis.
- 13. Lu, S., Fujii, H., Sugiyama, H., Tanaka, M., and Nogi, K. 2002. Weld penetration and Marangoni convection with oxide fluxes in GTA welding. Materials Transactions, Japan, 43(11): 2926-2931.
- 14. Yang, C., Lin, S., Liu, F., Wu, L., and Zhang, Q. 2003. Research on the mecha-

- nism of penetration increase by flux in A-TIG welding. Journal of Materials Science and Technology 19(1): 225-227.
- 15. Leconte, S., Paillard, P., Chapelle, P., Henrion, G., and Saindrenan, J. 2007. Effects of flux containing fluorides on TIG welding processes. Science and Technology of Welding and Joining 12(2): 120–126.
- 16. Howse, D. H., and Lucas, W. 2000. An investigation into arc constriction by active fluxes for TIG (A-TIG) welding. Science and Technology of Welding and Joining 5(3): 189-
- 17. Hiraoka. K. 1998. Plasma structures of Ar-H2 mixed gas tungsten arcs determined by spectroscopy measurements. Weld. Int. 12(3): 186-194.
- 18. Kobayashi, M., and Suga, T. 1979. A method for the spectral temperature measurement of a welding arc. Arc Physics and Weld Pool Behavior-International Conference Proceedings, London, UK. Ed. W. Lucas, Abington, UK: The Welding Institute, 1980, pp. 25-37.
- 19. Griem, H. R. 1997. Principles of Plasma Spectroscopy. Cambridge, UK: Cambridge University Press.
- 20. Lancaster, J. F. 1986. The Physics of Welding, 2nd Edition. International Institute of Welding.
- 21. Deutsch, M., and Beniaminy, I. 1982. Derivative-free inversion of Abel's integral equation. Appl. Phys. Lett. 41(1): 27, 28.
- 22. Liu, L. M., Cai, D. H., and Zhang, Z. D. 2007. Gas tungsten arc welding of magnesium alloy using activated flux-coated

- wire. Scripta Materialia, pp 57, 695-698.
- 23. Liu, L. M., Cai, D. H., and Zhang, Z. D. 2008. Magnesium alloy weld using manganese chloride coated wire. Science and Technology of Welding and Joining 13(1):
- 24. Matsushita, M. 2001. Clarification of hydrogen reduction mechanism in steel weld metal by means of fluoride additions in welding flux. Colorado School of Mines, Golden, Colo., PhD thesis.
- 25. Liu, S., and Perez, F. 2001. Manufacturing titanium flux-cored arc welding electrodes — Feasibility study. U.S. Navy Contract N00167- 01-M-0053, final re-
- 26. Handbook of Corrosion Data, 2nd edition. 1995. Materials Park, Ohio: ASM International.
- 27. Ferdjani et al. 1993. Anodic oxidation of titanium in phosphoric acid baths: Phosphorus incorporation into the oxide. Journal of Alloys and Compounds, 200: 191-194.
- 28. Krasicka-Cydzik, E. 2004. Gel-like layer development during formation of thin anodic films on titanium in phosphoric acid solutions. Corrosion Science 46: 2487-2502.
- 29. Narayanan, R., and Sesharderi, S. K. 2007. Phosphoric acid anodization of Ti-6Al-4V, Structural and corrosion aspects. Corrosion Science 49: 542-558.
- 30. http://cartech.ides.com/ datasheet.aspx?i=101&E=266. Sept. 25,

Call for Papers JOM-18

18th International Conference on Joining Materials Institute for the Joining of Materials in association with IIW Helsingør, Denmark, April 26-29, 2015

Download the brochure detailing topics, expenses, and registration form at:

www.aws.org/wj/JOM-18-CallForPapers.pdf

Review the brochure for conference topics. E-mail a title and short abstract of your paper before Nov. 2, 2014. You will receive author guidelines for preparation of the full paper by Nov. 30. The full paper for publication in the Conference Proceedings must be received by Jan. 15, 2015. E-mail to jom_aws@post10.tele.dk.









